arXiv:1408.1080v1 [cond-mat.stat-mech] 5 Aug 2014

Screening of an electrically charged particle in a two-dimensional two-component plasma at $\Gamma = 2$

Alejandro Ferrero[1] and Gabriel Téllez[2]

Departamento de Física
Universidad de los Andes
Bogotá, Colombia

Abstract

We consider the thermodynamic effects of an electrically charged impurity immersed in a two-dimensional two-component plasma, composed by particles with charges $\pm e$, at temperature T, at coupling $\Gamma = e^2/(k_B T) = 2$, confined in a large disk of radius R. Particularly, we focus on the analysis of the charge density, the correlation functions, and the grand potential. Our analytical results show how the charges are redistributed in the circular geometry considered here. When we consider a positively charged impurity, the negative ions accumulate close to the impurity leaving an excess of positive charge that accumulates at the boundary of the disk. Due to the symmetry under charge exchange, the opposite effect takes place when we place a negative impurity. Both the cases in which the impurity charge is an integer multiple of the particle charges in the plasma, $\pm e$, and a fraction of them are considered; both situations require a slightly different mathematical treatments, showing the effect of the quantization of plasma charges. The bulk and tension effects in the plasma described by the grand potential are not modified by the introduction of the charged particle. Besides the effects due to the collapse coming from the attraction between oppositely charged ions, an additional topological term appears in the grand potential, proportional to $-n^2 \ln(mR)$, with n the dimensionless charge of the particle. This term modifies the central charge of the system, from $c = 1$ to $c = 1 - 6n^2$, when considered in the context of conformal field theories.

[1] a.ferrero@uniandes.edu.co
[2] gtellez@uniandes.edu.co

1 Introduction

A two-dimensional two-component plasma (TCP) is a gas composed by two kinds of electrically charged particles (with charges $\pm e$) interacting through an electrostatic potential. In two dimensions, the Coulomb interaction between two unit charges separated by a distance r is $-\ln(r/L)$ with L an irrelevant length. The value of the charges, together with the inverse temperature factor $\beta = (k_B T)^{-1}$ determine a coupling constant given by $\Gamma = \beta e^2$.

The value of Γ is important to determine the behavior and stability of the system. For low temperatures ($\Gamma \geq 2$), the thermal energy is not enough to avoid the collapse of oppositely charged ions and the point particles must be replaced by hard disks of radius a. The point particle view, however, can still be kept when $\Gamma < 2$ because the thermal fluctuations allow to avoid such collapse. For the value $\Gamma = 2$, which we will assume in this analysis, the classical Coulomb gas is mathematically isomorph to a quantum free Fermi field at zero temperature [1]. Moreover, analytical solutions for the grand potential, densities and correlation functions can be found for this particular value of the coupling constant.

The analogy between the two-component plasma and the sine-Gordon quantum field theory has been exploited to obtain results for the thermodynamic properties of the Coulomb gas under some conditions when $\Gamma < 2$ [2, 3, 4]. When $\Gamma > 2$, an infinite-order transition that take place when $\Gamma = 4$ at low density (the Kosterlitz-Thouless transition) has been studied [5]; additionally, exact results for the plasma for values of Γ larger than 2, but close enough to 2, have also been found [6, 7].

In the particular case $\Gamma = 2$ several studies have been done in the past: the one-component plasma (a system composed by only one kind of particles immersed in an oppositely charged background) with adsorbing impurities [8, 9], and the two component plasma with adsorbing boundaries [10, 11] and adsorbing impurities [12].

In this work, we study the introduction of an electrically charged impurity into the plasma. The plasma occupies a disk region of radius R. The impurity is an impenetrable disk of radius r_0 and charge $q = ne$ located at the center of the disk domain that contains the plasma. The electrostatic potential generated by the impurity, at a distance r from it, can be written as $V(r) = -ne\ln(r/L)$, where n is the dimensionless charge of the impurity. From this point on, we will understand that the charge q of the impurity is "integer" if q is an integer multiple of e, i.e., $q = ne$, with $n \in \mathbb{Z}$. On the other hand, a "non-integer" charge means that $n \notin \mathbb{Z}$ and so there is a fractional part in the charge of the impurity that cannot be compensated by the other particles in the gas. Using the electrostatic potential just described, we can find the fugacities for positive and negative particles; they are

$$m_s(\mathbf{r}) = m(\mathbf{r})e^{-s\beta eV(r)} = m(\mathbf{r})\left(\frac{r}{L}\right)^{2sn}, \tag{1}$$

where $s = \pm 1$, and $m(\mathbf{r}) = 0$ for $|\mathbf{r}| = r < r_0$ and $m(\mathbf{r}) = m$ for $r > r_0$.

This model can be applied to some physical systems. The present concentrical circular geometry can be seen as a transversal cut of a cylindrical geometry. The location of the impurity at the center of the system generates the redistribution of charge that induces the accumulation of positive or negative ions around the impurity and the boundary of the plasma. Some proteins and other components in biological systems could be modeled as large cylinders with hard core effects and electrical charges spread along their length. To be able to describe the effective interactions between these charged entities immersed in an electrolyte is an important task towards understanding its physical properties.

Although the screening of charges in an electrolyte is fairly well understood in the mean field regime, $\Gamma \to 0$, described by the Poisson–Boltzmann equation [13, 14, 15], the intermediate and strong coupling regimes remain elusive. There has been several efforts towards the understanding of the strong coupling regime [16, 17, 18, 19, 20, 21]. However, most of the strong-coupling techniques, such as the Wigner strong coupling approach [19, 20], are only targeted at the one-component plasma, and cannot directly be applied to a multicomponent plasma such as the one studied here. Thus, the present work tries to contribute to the understanding of the screening beyond the mean field by studying the intermediate coupling $\Gamma = 2$.

There has been previous studies of charged impurities in the two-dimensional two-component plasma beyond mean field, for $0 < \Gamma < 2$, but limited to point impurities in the bulk. In these works, the use of the form factors of the sine-Gordon field theory allows to obtain the behavior of the density profiles at large distances from the impurity [22] and using the product operator expansion, one can obtain the short distance behavior of the densities [23]. However, the complete form of the density profiles for the whole range of distances is unknown. At $\Gamma = 2$, the equivalent field theory to the two-component plasma is a free fermion one, therefore it will be possible to obtain more explicit results in the present case, and also consider the effets of the nonzero size of the impurity ($r_0 \neq 0$), and the confinement of the plasma ($R < \infty$).

This paper is organized as follows: in section 2 we briefly discuss the theoretical background for a two-dimensional two-component plasma at $\Gamma = 2$. Section 3 discusses the Green's functions that generate the density and correlations of the plasma. The density of the gas and the total charge are discussed in sections 4 and 5 respectively. Chapter 6 explains the calculation of the grand potential. We finally summarize our conclusions and discuss the results in section 7.

2 Formalism

In 1989, Cornu and Jancovici developed a general formalism to study a two-dimensional two-component gas at $\Gamma = e^2\beta = 2$ [1]. Within this model, the two-dimensional position of a particle $\mathbf{r} = (x, y)$ can be written in complex coordinates as $z = x + iy$. As explained before, when $\Gamma = 2$ the point particles must be replaced by hard spheres of radius a; its

inverse a^{-1} could also be viewed as an ultraviolet cutoff in momentum space. In the limit $a \to 0$, the logarithm of the grand partition function Ξ for this system takes the form [1]

$$\ln \Xi = \mathrm{Tr}\left[\ln\left(\not{\partial} + m_+(\mathbf{r})\frac{1+\sigma_z}{2} + m_-(\mathbf{r})\frac{1-\sigma_z}{2}\right) - \ln\,\not{\partial}\right]. \tag{2}$$

In a two-dimensional system, $\not{\partial} = \sigma_x\partial_x + \sigma_y\partial_y$, where σ_x, σ_y and σ_z are the Pauli matrices. The terms $m_\pm(\mathbf{r}) = m(\mathbf{r})e^{-\beta U_\pm(\mathbf{r})}$ are fugacities that take into account the effects of an electric external potential that generates electrostatic energies given by $U_\pm(r)$ for positive and negative particles. The term $m(\mathbf{r})$ includes hard-core effects and other non-electrical contributions. The calculation of the grand potential, $\Omega = -k_BT\ln\Xi$, is performed by finding the eigenvalues $\{\lambda_k\}$ of the system [1]

$$\left[\not{\partial} - \frac{1}{\lambda}\begin{pmatrix} m_+(\mathbf{r}) & 0 \\ 0 & m_-(\mathbf{r}) \end{pmatrix}\right]\psi(\mathbf{r}) = 0, \;\; \text{with} \;\; \psi(\mathbf{r}) = \begin{pmatrix} g(\mathbf{r}) \\ f(\mathbf{r}) \end{pmatrix} \tag{3}$$

a two-component spinor. Then the grand potential is given by

$$\beta\Omega = -\sum_k \ln(1+\lambda_k). \tag{4}$$

These two last equations show the equivalence between this system and a free Fermi gas [1]. The pressure p, in the thermodynamic limit, is given by

$$\beta p = \frac{\partial \ln\Xi}{\partial A} = -\frac{1}{A}\beta\Omega, \tag{5}$$

where A is the area of the gas. The truncated p-body densities are given by:

$$\begin{aligned} \rho^{(p)T}_{s_1,s_2\ldots s_p}(\mathbf{r}_1,\mathbf{r}_2,\ldots,\mathbf{r}_p) &= (-1)^{p+1}m_{s_1}(\mathbf{r}_1)m_{s_2}(\mathbf{r}_2)\ldots m_{s_p}(\mathbf{r}_p) \\ &\times \sum_{i_1,i_2\ldots,i_p} G_{s_{i_1},s_{i_2}}(\mathbf{r}_{i_1},\mathbf{r}_{i_2})\ldots G_{s_{i_p},s_{i_1}}(\mathbf{r}_{i_p},\mathbf{r}_{i_1}), \end{aligned} \tag{6}$$

where the summations run over cycles $\{i_1, i_2\ldots, i_n\}$. $G_{s_1s_2}(\mathbf{r}_1,\mathbf{r}_2)$ are matrix elements that satisfy the set of differential equations

$$\begin{pmatrix} m_+(\mathbf{r}_1) & 2\partial_{z_1} \\ 2\partial_{\bar{z}_1} & m_-(\mathbf{r}_1) \end{pmatrix}\begin{pmatrix} G_{++}(\mathbf{r}_1,\mathbf{r}_2) & G_{+-}(\mathbf{r}_1,\mathbf{r}_2) \\ G_{-+}(\mathbf{r}_1,\mathbf{r}_2) & G_{--}(\mathbf{r}_1,\mathbf{r}_2) \end{pmatrix} = \delta(\mathbf{r}_1-\mathbf{r}_2). \tag{7}$$

For the particular cases $n = 1$ and $n = 2$ we have

$$\begin{aligned} \rho^{(1)}_s(\mathbf{r}) &= m_s(\mathbf{r})G_{ss}(\mathbf{r},\mathbf{r}), \\ \rho^{(2)T}_{s_1s_2}(\mathbf{r}_1,\mathbf{r}_2) &= -m_{s_1}(\mathbf{r}_1)m_{s_2}(\mathbf{r}_2)G_{s_1s_2}(\mathbf{r}_1,\mathbf{r}_2)G_{s_2s_1}(\mathbf{r}_2,\mathbf{r}_1). \end{aligned} \tag{8}$$

Since the gas is not stable under the collapse of particles of opposite signs, the results will depend on the cutoff distance given by a. While the limit $a \to 0$ can be taken for some quantities such as the correlation functions, the charge density and other quantities will depend on such distance.

3 The Green functions

We will now study the effects of a charged particle of radius r_0 located at the center of the plasma with a potential given by $U(r) = -ne^2 \ln(r/L)$. This particle is thus immersed in a large electrical system confined in a large disk of radius R. Defining $g_{s_1 s_2} = e^{-is_1 U(r_1)} G_{s_1 s_2} e^{-is_2 U(r_2)}$ and using Eq. (7), we obtain the set of differential equations (for $r_0 < r < R$)

$$\left\{ m^2 - \nabla_1^2 - \frac{2in}{r_1^2}\frac{\partial}{\partial\theta_1} + \frac{n^2}{r_1^2} \right\} g_{\pm\pm}(\mathbf{r}_1, \mathbf{r}_2) = m\delta(\mathbf{r}_1 - \mathbf{r}_2), \tag{9}$$

$$g_{-+}(\mathbf{r}_1, \mathbf{r}_2) = -m^{-1} \left[2\partial_{\bar{z}_1} - n\frac{e^{i\theta_1}}{r_1} \right] g_{++}(\mathbf{r}_1, \mathbf{r}_2), \tag{10}$$

$$g_{+-}(\mathbf{r}_1, \mathbf{r}_2) = -m^{-1} \left[2\partial_{z_1} + n\frac{e^{-i\theta_1}}{r_1} \right] g_{--}(\mathbf{r}_1, \mathbf{r}_2). \tag{11}$$

We now propose a particular solution in terms of a Fourier expansion with l-modes $g^l_{ss'}(\mathbf{r}_1, \mathbf{r}_2) = e^{il\theta_1} g^l_{ss'}(\tilde{r}_1, \tilde{\mathbf{r}}_2)$, where we defined the dimensionless variables $\tilde{r}_{1,2} = mr_{1,2}$. In terms of these variables and using the stated Fourier decomposition, we see that the modes $g^l_{ss'}(\tilde{r}_1, \tilde{\mathbf{r}}_2)$ obey the differential equations

$$\left\{ \tilde{r}_1^2 \frac{d}{d\tilde{r}_1^2} + \tilde{r}_1 \frac{d}{d\tilde{r}_1} - \left[(l+n)^2 + \tilde{r}_1^2 \right] \right\} g^l_{\pm\pm}(\tilde{r}_1, \tilde{\mathbf{r}}_2) = m\delta(\tilde{r}_1 - \tilde{r}_2) e^{-il\theta_2}, \tag{12}$$

$$g^l_{-+}(\tilde{r}_1, \tilde{\mathbf{r}}_2) = -e^{i\theta_1} \left[\frac{d}{d\tilde{r}_1} - \frac{1}{\tilde{r}_1}(l+n) \right] g_{++}(\tilde{r}_1, \tilde{\mathbf{r}}_2), \tag{13}$$

$$g^l_{+-}(\tilde{r}_1, \tilde{\mathbf{r}}_2) = -e^{-i\theta_1} \left[\frac{d}{d\tilde{r}_1} + \frac{1}{\tilde{r}_1}(l+n) \right] g_{--}(\tilde{r}_1, \tilde{\mathbf{r}}_2). \tag{14}$$

The Fourier modes can thus be written in the form $g^l_{\pm\pm}(\tilde{r}_1, \tilde{\mathbf{r}}_2) = A_l(\tilde{\mathbf{r}}_2) K_{l+n}(\tilde{r}_1) + B_l(\tilde{\mathbf{r}}_2) I_{l+n}(\tilde{r}_1)$, where $I_l(x)$ and $K_l(x)$ are the modified Bessel functions of first and second kind and $A_l(\tilde{\mathbf{r}}_2)$ and $B_l(\tilde{\mathbf{r}}_2)$ are coefficients to be determined by the boundary conditions. We thus have (for $r_0 < r_1 < R$ and $r_1 < r_2$)

$$g_{\pm\pm} = \sum_l e^{il\theta_1} \left[A_l^{(\pm\pm)} K_{l+n}(\tilde{r}_1) + B_l^{(\pm\pm)} I_{l+n}(\tilde{r}_1) \right], \tag{15}$$

$$g_{\mp\pm} = \sum_l e^{i(l\pm1)\theta_1} \left[A_l^{(\pm\pm)} K_{l+n\pm1}(\tilde{r}_1) - B_l^{(\pm\pm)} I_{l+n\pm1}(\tilde{r}_1) \right], \tag{16}$$

and something similar for $r_2 < r_1$ where the coefficients for that region will be called $A_l'^{(\pm\pm)}$ and $B_l'^{(\pm\pm)}$.

In the regions $r < r_0$ and $r > R$ we have that the fugacity vanishes so $m = 0$. Therefore, the differential equations for $G_{s_1 s_2}$ imply that

$$G^l_{++} = u^{(++)}_l e^{il\theta_1} r_1^l, \quad G^l_{+-} = u^{(+-)}_l e^{i(l-1)\theta_1} r_1^{l-1}, \tag{17}$$

$$G^l_{--} = u^{(--)}_l e^{il\theta_1} r_1^{-l}, \quad G^l_{-+} = u^{(-+)}_l e^{i(l+1)\theta_1} r_1^{-(l+1)}, \tag{18}$$

where the coefficients $u^{(s_1 s_2)}_l$ have to be determined for each one of the two regions. Eqs. (12)−(14), (17) and (18) imply the following boundary conditions:

1. $g_{\pm\pm}$ must be continuous at $r_1 = r_2$.
2. $g_{\pm\mp}$ must be discontinuous at $r_1 = r_2$.
3. $G_{s_1 s_2}$ must be finite at $r = 0$.
4. $G_{s_1 s_2}$ must vanish at $r = \infty$.

While the first and the second conditions are given by the delta distribution in Eq. (12) and provide relations for the coefficients A_l and B_l in the regions $r_0 < r_{1,2} < R$, the third and fourth conditions provide the extra conditions by stating which $u^{(s_1 s_2)}_l$ coefficients must vanish.

From now on we will use the notations $F(\tilde{r}_j) \equiv F^{(j)}$ and $F(\tilde{R}) \equiv F^{(R)}$. The continuity conditions at $r_1 = r_0$ imply

$$A^{(--)}_l K^{(0)}_{l+n} + B^{(--)}_l I^{(0)}_{l+n} = 0, \;\; l \geq 1, \tag{19}$$

$$A^{(--)}_l K^{(0)}_{l+n-1} - B^{(--)}_l I^{(0)}_{l+n-1} = 0, \;\; l \leq 0, \tag{20}$$

$$A^{(++)}_l K^{(0)}_{l+n+1} - B^{(++)}_l I^{(0)}_{l+n+1} = 0, \;\; l \geq 0, \tag{21}$$

$$A^{(++)}_l K^{(0)}_{l+n} + B^{(++)}_l I^{(0)}_{l+n} = 0, \;\; l \leq -1. \tag{22}$$

Additionally, the continuity conditions at $r_1 = R$ demand:

$$A'^{(--)}_l K^{(R)}_{l+n} + B'^{(--)}_l I^{(R)}_{l+n} = 0, \;\; l \leq 0, \tag{23}$$

$$A'^{(--)}_l K^{(R)}_{l+n-1} - B'^{(--)}_l I^{(R)}_{l+n-1} = 0, \;\; l - 1 \geq 0, \tag{24}$$

$$A'^{(++)}_l K^{(R)}_{l+n+1} - B'^{(++)}_l I^{(R)}_{l+n+1} = 0, \;\; l + 1 \leq 0, \tag{25}$$

$$A'^{(++)}_l K^{(R)}_{l+n} + B'^{(++)}_l I^{(R)}_{l+n} = 0, \;\; l \geq 0. \tag{26}$$

On the other hand, the two conditions at $r_1 = r_2$ are

$$A^{(\pm\pm)}_l K^{(2)}_{l+n} + B^{(\pm\pm)}_l I^{(2)}_{l+n} - A'^{(\pm\pm)}_l K^{(2)}_{l+n} - B'^{(\pm\pm)}_l I^{(2)}_{l+n} = 0, \tag{27}$$

$$A'^{(\pm\pm)}_l K^{(2)}_{l+n\pm1} - A^{(\pm\pm)}_l K^{(2)}_{l+n\pm1} - B'^{(\pm\pm)}_l I^{(2)}_{l+n\pm1} + B^{(\pm\pm)}_l I^{(2)}_{l+n\pm1} = \frac{m}{2\pi\tilde{r}_2} e^{-il\theta_2}. \tag{28}$$

The particular Green functions are thus found by solving for the coefficients given in Eqs. (19)−(28). Using the definitions

$$t_l^{(x)} \equiv \frac{K_l(x)}{I_l(x)}\,, \tag{29}$$

and $\theta_{12} \equiv \theta_1 - \theta_2$, and writing n as $n = k+\nu$, where k and ν are the integer and fractional parts of n respectively, we find

$$g_{++} = \frac{m}{2\pi} e^{-ik\theta_{12}} \Big[\sum_l e^{il\theta_{12}} I^{(<)}_{l+\nu} K^{(>)}_{l+\nu} + \Delta_{++}^{(\nu,\tilde{r}_0,\tilde{R})} \Big], \tag{30}$$

$$g_{--} = \frac{m}{2\pi} e^{-ik\theta_{12}} \Big[\sum_l e^{il\theta_{12}} I^{(<)}_{l+\nu} K^{(>)}_{l+\nu} + \Delta_{--}^{(\nu,\tilde{r}_0,\tilde{R})} \Big], \tag{31}$$

where the notation $(<)$ and $(>)$ means that we choose between the smaller and larger between r_1 and r_2 respectively and

$$\begin{aligned}
\Delta_{++}^{(\nu,\tilde{r}_0,\tilde{R})} = &- \sum_{l=-\infty}^{k-1} e^{il\theta_{12}} \frac{[t^{(0)}_{l+\nu}]^{-1} K^{(1)}_{l+\nu} K^{(2)}_{l+\nu}}{1 + [t^{(0)}_{l+\nu}]^{-1} t^{(R)}_{l+\nu+1}} + \sum_{l=k}^{\infty} e^{il\theta_{12}} \frac{[t^{(0)}_{l+\nu+1}]^{-1} K^{(1)}_{l+\nu} K^{(2)}_{l+\nu}}{1 + [t^{(0)}_{l+\nu+1}]^{-1} t^{(R)}_{l+\nu}} \\
&- \sum_{l=-\infty}^{k-1} e^{il\theta_{12}} t^{(R)}_{l+\nu+1} \frac{[t^{(0)}_{l+\nu}]^{-1} (I^{(1)}_{l+\nu} K^{(2)}_{l+\nu} + K^{(1)}_{l+\nu} I^{(2)}_{l+\nu}) - I^{(1)}_{l+\nu} I^{(2)}_{l+\nu}}{1 + [t^{(0)}_{l+\nu}]^{-1} t^{(R)}_{l+\nu+1}} \\
&- \sum_{l=k}^{\infty} e^{il\theta_{12}} t^{(R)}_{l+\nu} \frac{[t^{(0)}_{l+\nu+1}]^{-1} (I^{(1)}_{l+\nu} K^{(2)}_{l+\nu} + K^{(1)}_{l+\nu} I^{(2)}_{l+\nu}) + I^{(1)}_{l+\nu} I^{(2)}_{l+\nu}}{1 + [t^{(0)}_{l+\nu+1}]^{-1} t^{(R)}_{l+\nu}},
\end{aligned} \tag{32}$$

$$\begin{aligned}
\Delta_{--}^{(\nu,\tilde{r}_0,\tilde{R})} = &\sum_{l=-\infty}^{k} e^{il\theta_{12}} \frac{[t^{(0)}_{l+\nu-1}]^{-1} K^{(1)}_{l+\nu} K^{(2)}_{l+\nu}}{1 + [t^{(0)}_{l+\nu-1}]^{-1} t^{(R)}_{l+\nu}} - \sum_{l=k+1}^{\infty} e^{il\theta_{12}} \frac{[t^{(0)}_{l+\nu}]^{-1} K^{(1)}_{l+\nu} K^{(2)}_{l+\nu}}{1 + [t^{(0)}_{l+\nu}]^{-1} t^{(R)}_{l+\nu-1}} \\
&- \sum_{l=-\infty}^{k} e^{il\theta_{12}} t^{(R)}_{l+\nu} \frac{[t^{(0)}_{l+\nu-1}]^{-1} (I^{(1)}_{l+\nu} K^{(2)}_{l+\nu} + K^{(1)}_{l+\nu} I^{(2)}_{l+\nu}) + I^{(1)}_{l+\nu} I^{(2)}_{l+\nu}}{1 + [t^{(0)}_{l+\nu-1}]^{-1} t^{(R)}_{l+\nu}} \\
&- \sum_{l=k+1}^{\infty} e^{il\theta_{12}} t^{(R)}_{l+\nu-1} \frac{[t^{(0)}_{l+\nu}]^{-1} (I^{(1)}_{l+\nu} K^{(2)}_{l+\nu} + K^{(1)}_{l+\nu} I^{(2)}_{l+\nu}) - I^{(1)}_{l+\nu} I^{(2)}_{l+\nu}}{1 + [t^{(0)}_{l+\nu}]^{-1} t^{(R)}_{l+\nu-1}}.
\end{aligned} \tag{33}$$

The functions $g_{\pm\mp}$ are found using Eqs. (13) and (14).

From this point we should emphasize the difference between the cases $n \in \mathbb{Z}$ ($\nu = 0$) and $n \notin \mathbb{Z}$ ($\nu \neq 0$). Mathematically, when $l \in \mathbb{Z}$, $I_l(x) = I_{-l}(x)$ but $I_{-(l+\nu)}(x) = I_{l+\nu}(x) + d^l_\nu K_{l+\nu}(x)$, with $d^l_\nu \equiv \frac{2}{\pi}(-1)^l \sin(\pi\nu)$.

Up to a phase factor, the term $\frac{m}{2\pi}\sum_l e^{il\theta_{12}} I^{(<)}_{l+\nu} K^{(>)}_{l+\nu}$ in last equations reproduces the contribution for the unperturbed plasma $g^0_{ss'}(\mathbf{r}_1, \mathbf{r}_2) = \frac{m}{2\pi} K_0(|\tilde{r}_1 - \tilde{r}_2|)$ in the case $\nu = 0$. For $\nu \neq 0$ we separate this term by writing

$$\frac{m}{2\pi} \sum_l e^{il\theta_{12}} I^{(<)}_{l+\nu} K^{(>)}_{l+\nu} = g^0_{ss'}(\mathbf{r}_1, \mathbf{r}_2) + \frac{m}{2\pi} \sum_l e^{il\theta_{12}} (I^{(<)}_{l+\nu} K^{(>)}_{l+\nu} - I^{(<)}_l K^{(>)}_l). \tag{34}$$

The remaining contributions, defined as $\Delta_{s_1 s_2}^{(\nu,\tilde{r}_0,\tilde{R})}$, depend on ν, r_0 and R and describe effects purely generated by the impurity.

4 Density Profile

The density of the positive and negative particles in the plasma can easily be evaluated using the Green's functions found in the previous section. Using Eq. (6), we can verify that

$$\rho_{\pm}(\mathbf{r}) = m g_{\pm\pm}(\mathbf{r},\mathbf{r}). \tag{35}$$

We can also define the charge density (divided by e), $\rho_t(\mathbf{r})$, as the difference between the density of positive and negative particles; it is given by

$$\rho_t(\mathbf{r}) = m[\, g_{++}(\mathbf{r},\mathbf{r}) - g_{--}(\mathbf{r},\mathbf{r})\,]. \tag{36}$$

Since the case $\nu = 0$ is a particular situation of the more general case $\nu \neq 0$, we will assume the most general situation and use the limit $\nu \to 0$ in order to find the solutions for the particular case in which the impurity has an integer charge. Remember that in the unperturbed case $\rho_{\pm}^0(\mathbf{r}) \equiv \rho^0 \underset{a\to 0}{=} \dfrac{m^2}{2\pi}\left(\ln\dfrac{2}{ma} - \gamma\right) + O(1)$ [1], where a is the cutoff and γ is the Euler-Mascheroni constant.

4.1 General Case

The density profile can be found using Eqs. (32)−(36). For computational reasons it is better to eliminate the negative modes in Eqs. (32) and (33) in favor of only positive ones. Using $I_{-(l+\nu)}(x) = I_{l+\nu}(x) + d_\nu^l K_{l+\nu}(x)$ we notice that

$$[t_{-l+\nu}^{(0)}]^{-1} = [t_{l-\nu}^{(0)}]^{-1} - d_\nu^l, \qquad t_{-l+\nu+1}^{(R)} = \frac{t_{l-\nu-1}^{(R)}}{1 + d_\nu^l t_{l-\nu-1}^{(R)}}. \tag{37}$$

We use a definition for ν in which $-1 < \nu < 1$. For example, if $n = 7/2$ we have that $k = 3$ and $\nu = 1/2$, but for $n = -7/2$ we have $k = -3$ and $\nu = -1/2$. We thus use the

notation $\nu_\pm$ to indicate the cases when $n \geq 0$ and $n < 0$ respectively. Then we find

$$\begin{aligned}
\frac{2\pi}{m^2}\rho_+^{(\nu_+,\tilde{r}_0,\tilde{R})}(\mathbf{r}) = \frac{2\pi}{m^2}\tilde{\rho}_\nu^0 &- \sum_{l=0}^{k-1}\frac{[t_{l+\nu}^{(0)}]^{-1}[\,K_{l+\nu}^{(r)}]^2}{1+[t_{l+\nu}^{(0)}]^{-1}t_{l+\nu+1}^{(R)}} - \sum_{l=0}^{k-1} t_{l+\nu+1}^{(R)}\frac{2[t_{l+\nu}^{(0)}]^{-1}I_{l+\nu}^{(r)}K_{l+\nu}^{(r)} - [\,I_{l+\nu}^{(r)}]^2}{1+[t_{l+\nu}^{(0)}]^{-1}t_{l+\nu+1}^{(R)}} \\
&- \sum_{l=1}^{\infty}\frac{[t_{l-\nu}^{(0)}]^{-1}[\,K_{l-\nu}^{(r)}]^2}{1+[t_{l-\nu}^{(0)}]^{-1}t_{l-\nu-1}^{(R)}} - \sum_{l=1}^{\infty} t_{l-\nu-1}^{(R)}\frac{2[t_{l-\nu}^{(0)}]^{-1}I_{l-\nu}^{(r)}K_{l-\nu}^{(r)} - [\,I_{l-\nu}^{(r)}]^2}{1+[t_{l-\nu}^{(0)}]^{-1}t_{l-\nu-1}^{(R)}} \\
&+ \sum_{l=k}^{\infty}\frac{[t_{l+\nu+1}^{(0)}]^{-1}[\,K_{l+\nu}^{(r)}]^2}{1+[t_{l+\nu+1}^{(0)}]^{-1}t_{l+\nu}^{(R)}} - \sum_{l=k}^{\infty} t_{l+\nu}^{(R)}\frac{2[t_{l+\nu+1}^{(0)}]^{-1}I_{l+\nu}^{(r)}K_{l+\nu}^{(r)} + [\,I_{l+\nu}^{(r)}]^2}{1+[t_{l+\nu+1}^{(0)}]^{-1}t_{l+\nu}^{(R)}}, \qquad (38)
\end{aligned}$$

$$\begin{aligned}
\frac{2\pi}{m^2}\rho_-^{(\nu_+,\tilde{r}_0,\tilde{R})}(\mathbf{r}) = \frac{2\pi}{m^2}\tilde{\rho}_\nu^0 &+ \sum_{l=0}^{k}\frac{[t_{l+\nu-1}^{(0)}]^{-1}[\,K_{l+\nu}^{(r)}]^2}{1+[t_{l+\nu-1}^{(0)}]^{-1}t_{l+\nu}^{(R)}} - \sum_{l=0}^{k} t_{l+\nu}^{(R)}\frac{2[t_{l+\nu-1}^{(0)}]^{-1}I_{l+\nu}^{(r)}K_{l+\nu}^{(r)} + [\,I_{l+\nu}^{(r)}]^2}{1+[t_{l+\nu-1}^{(0)}]^{-1}t_{l+\nu}^{(R)}} \\
&+ \sum_{l=1}^{\infty}\frac{[t_{l-\nu+1}^{(0)}]^{-1}[\,K_{l-\nu}^{(r)}]^2}{1+[t_{l-\nu+1}^{(0)}]^{-1}t_{l-\nu}^{(R)}} - \sum_{l=1}^{\infty} t_{l-\nu}^{(R)}\frac{2[t_{l-\nu+1}^{(0)}]^{-1}I_{l-\nu}^{(r)}K_{l-\nu}^{(r)} + [\,I_{l-\nu}^{(r)}]^2}{1+[t_{l-\nu+1}^{(0)}]^{-1}t_{l-\nu}^{(R)}} \\
&- \sum_{l=k+1}^{\infty}\frac{[t_{l+\nu}^{(0)}]^{-1}[\,K_{l+\nu}^{(r)}]^2}{1+[t_{l+\nu}^{(0)}]^{-1}t_{l+\nu-1}^{(R)}} - \sum_{l=k+1}^{\infty} t_{l+\nu-1}^{(R)}\frac{2[t_{l+\nu}^{(0)}]^{-1}I_{l+\nu}^{(r)}K_{l+\nu}^{(r)} - [\,I_{l+\nu}^{(r)}]^2}{1+[t_{l+\nu}^{(0)}]^{-1}t_{l+\nu-1}^{(R)}}, \qquad (39)
\end{aligned}$$

with

$$\tilde{\rho}_\nu^0 = \frac{m^2}{2\pi}\sum_{l=0}^{\infty} I_{l+\nu}^{(r)}K_{l+\nu}^{(r)} + \frac{m^2}{2\pi}\sum_{l=1}^{\infty} I_{l-\nu}^{(r)}K_{l-\nu}^{(r)}. \qquad (40)$$

When $\nu < 0$ we can obtain the solutions using the symmetry relations $\rho_+(\nu_+,k) = \rho_-(-\nu_-,-k)$ and $\rho_+(-\nu_-,-k) = \rho_-(\nu_+,k)$. Notice that $\tilde{\rho}_0^0 = \rho^0$ when $\nu = 0$.

Figures 1, 2, 3 and 4 show the density of positive and negative particles for different values of charge impurity $n > 0$. The density of positive particles vanishes near r_0 due to the repulsive interaction with the impurity carrying a positive charge. On the contrary the density of negative particles increases in an effort to screen the impurity. Far from the impurity both densities converge to the bulk density ρ^0. For $n < 1$, the behavior of the negative density in the presence of a fractional impurity presents an interesting effect which takes place near r_0 approaching it from above (see figure 4). The amount of negative ions slightly decreases after taking a maximum value in the neighborhood of the impurity. This behavior is more notable for smaller values of ν. This effect, however, seems to be a property satisfied only by charges $n < 1$ and not by any non-integer impurity; as can be seen in figure 2, such behavior is absent for $n = 2.1$. The electrostatic interaction between the impurity and a negative charge of the plasma can be caracterized by a coupling constant given by $\Gamma_n = n\beta e^2$ (see table 1 for more details). If the impurity radius is very small $r_0 \to 0$, then when $n \geq 1$ ($\Gamma_n \geq 2$) there will be a collapse of the negative particles against the charged impurity, therefore a very large value of $\rho_-(r)$ as $r \to 0$. On the other hand, if $n < 1$ the system is stable against that collapse and so the

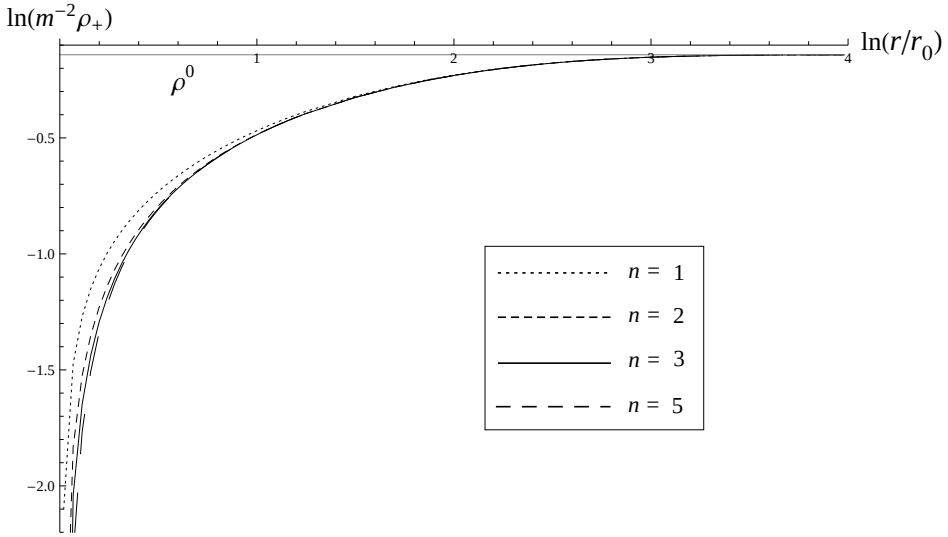

Figure 1: Density of the positive charge for four different integer impurities located at the origin. The size of the impurity is $mr_0 = 0.05$ and the size of the disk is $mR = 30$. The density becomes zero as $r \to r_0$. We used $m^{-2}\rho^0 = 0.87$.

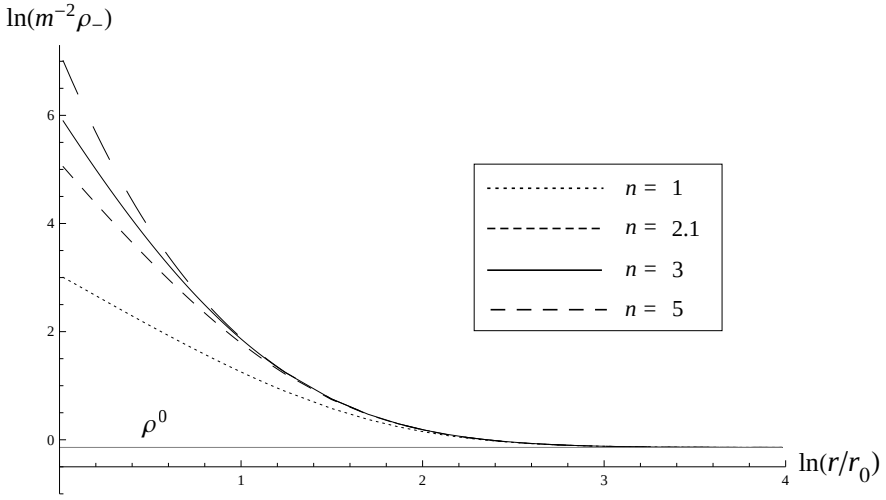

Figure 2: Density of the negative charge for four different impurities located at the origin. The size of the impurity is $mr_0 = 0.05$ and the size of the disk is $mR = 30$. We used $m^{-2}\rho^0 = 0.87$.

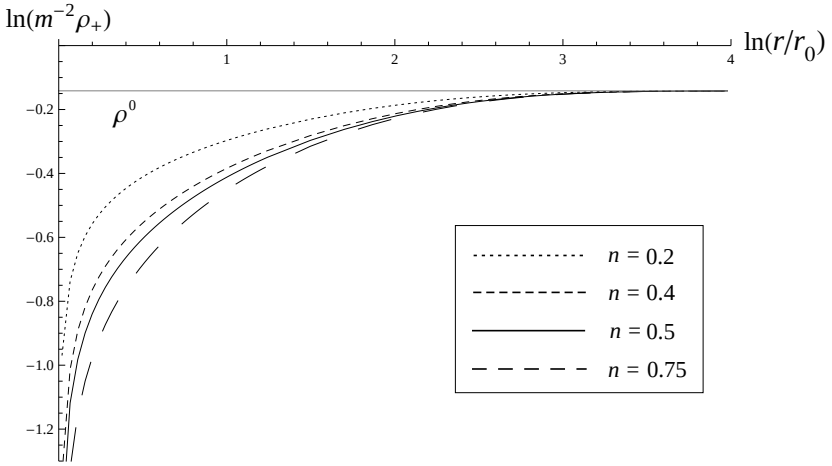

Figure 3: Density of the positive charge for four different fractional impurities located at the origin. The size of the impurity is $mr_0 = 0.05$ and the size of the disk is $mR = 30$. We used $m^{-2}\rho^0 = 0.87$.

value of the negative density at the origin decreases. (Such behavior is described in table 2.) A fingerprint of these two regimes can be seen in figures 2, 4 and 5 which show a change of behavior in the density when the impurity charge changes from $n < 1$ to $n > 1$. A similar observation was made in the analysis when $r_0 = 0$ and $\Gamma < 2$ [23]. Although such results are restricted for $\Gamma < 2$ and $r_0 = 0$, the negative density for small r in the case $\Gamma \to 2^-$ would take the form [23]

$$\rho_-(r) \underset{r\to 0}{=} A_1 r^{-2n} + O(r^{2(1-n)}), \qquad \text{for } n < 1\,, \tag{41}$$

where A_1 is a constant. The results shown in table 1 match last predictions in the case $n < 1$ and $r_0 \to 0$, ie. $\rho_-(r) \propto r^{-2n}$. When $n > 1$, this behavior changes, in part due to the collapse of the negative ions into the charged impurity.

4.2 Asymptotic limits

It is interesting to study the limiting cases in which $r_0 \to 0$ and $R \to \infty$. When $r_0 \to 0$ we have that $[t^{(0)}_{l+\nu}]^{-1} \sim \frac{2}{\Gamma(l+\nu)\Gamma(l+\nu+1)} \left(\frac{r_0}{2}\right)^{2(l+\nu)}$ for $l > 0$ and $[t^{(0)}_0]^{-1} \sim \frac{2(1-\delta_{0\nu})}{\Gamma(\nu)\Gamma(\nu+1)} \left(\frac{r_0}{2}\right)^{2\nu} + \frac{m^2}{2\pi}\frac{\delta_{0\nu}}{\rho^0(r_0)}$, where $\rho^0(r_0) = \rho^0(a = r_0)$, for $l = 0$. Although such terms vanish as $r_0 \to 0$, a term of the form $[t^{(0)}_{l+\nu}]^{-1}[K^{(r)}_{l+\nu}]^2$ does not necessarily cancel for small values of r because $K^{(r)}_{l+\nu}$ diverges. These contributions can be neglected, however, when $r \gg r_0$; in this limit

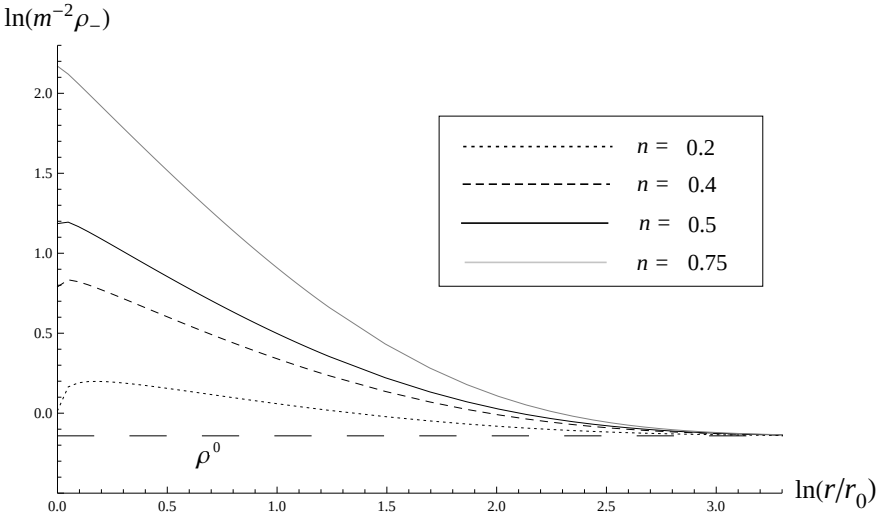

Figure 4: Density of the negative charge for four different fractional impurities located at the origin. The size of the impurity is $mr_0 = 0.05$ and the size of the disk is $mR = 30$. We used $m^{-2}\rho^0 = 0.87$.

we have

$$\frac{2\pi}{m^2}\rho_+^{(\nu_+,0,\tilde{R})}(\mathbf{r}) = \frac{2\pi}{m^2}\tilde{\rho}_\nu^0 + \sum_{l=1}^{\infty} t_{l-\nu-1}^{(R)}[\,I_{l-\nu}^{(r)}]^2 + \sum_{l=1}^{k-1} t_{l+\nu+1}^{(R)}[\,I_{l+\nu}^{(r)}]^2 - \sum_{l=k}^{\infty} t_{l+\nu}^{(R)}[\,I_{l+\nu}^{(r)}]^2$$
$$- (1-\delta_{0k})\frac{\frac{m^2}{2\pi}\frac{\delta_{0\nu}}{\rho^0(r_0)}[K_0^{(r)}]^2}{1+\frac{m^2}{2\pi}\frac{\delta_{0\nu}}{\rho^0(r_0)}t_1^{(R)}} - (1-\delta_{0k})t_{1+\nu}^{(R)}\frac{\frac{2m^2}{2\pi}\frac{\delta_{0\nu}}{\rho^0(r_0)}I_0^{(r)}K_0^{(r)} - [I_\nu^{(r)}]^2}{1+\frac{m^2}{2\pi}\frac{\delta_{0\nu}}{\rho^0(r_0)}t_1^{(R)}}, \quad (42)$$

$$\frac{2\pi}{m^2}\rho_-^{(\nu_+,0,\tilde{R})}(\mathbf{r}) = \frac{2\pi}{m^2}\tilde{\rho}_\nu^0 - \sum_{l=1}^{\infty} t_{l-\nu}^{(R)}[\,I_{l-\nu}^{(r)}]^2 - \sum_{l=2}^{k} t_{l+\nu}^{(R)}[\,I_{l+\nu}^{(r)}]^2 + \sum_{l=k+1}^{\infty} t_{l+\nu-1}^{(R)}[\,I_{l+\nu}^{(r)}]^2$$
$$- t_\nu^{(R)}\frac{2d_\nu^0 I_\nu^{(r)}K_\nu^{(r)} + [I_\nu^{(r)}]^2}{1+d_\nu^0 t_\nu^{(R)}} - (1-\delta_{0k})t_{1+\nu}^{(R)}\frac{\frac{2m^2}{2\pi}\frac{\delta_{0\nu}}{\rho^0(r_0)}I_1^{(r)}K_1^{(r)} + [I_{1+\nu}^{(r)}]^2}{1+\frac{m^2}{2\pi}\frac{\delta_{0\nu}}{\rho^0(r_0)}t_1^{(R)}}$$
$$+ \frac{d_\nu^0[K_\nu^{(r)}]^2}{1+d_\nu^0 t_\nu^{(R)}} + (1-\delta_{0k})\frac{\frac{m^2}{2\pi}\frac{\delta_{0\nu}}{\rho^0(r_0)}[K_1^{(r)}]^2}{1+\frac{m^2}{2\pi}\frac{\delta_{0\nu}}{\rho^0(r_0)}t_1^{(R)}}. \quad (43)$$

Another interesting limit is the case $R \to \infty$. In this limit $t_{l+\nu}^{(R)} \to 0$ but terms of the form $t_l^{(R)}[I_l^{(r)}]^2$ do not necessarily vanish as $r \to \infty$. However, if we consider the case $r \ll R$

mr_0	n											
	7	5.2	4	3.5	2.7	2	1.4	1	0.8	0.6	0.4	0.2
10^{-1}	-8.92	-7.25	-5.88	-5.33	-4.37	-3.43	-2.47	-1.65	-1.23	-0.81	-0.40	-0.12
10^{-3}	-9.11	-7.42	-6.13	-5.52	-4.65	-3.81	-2.80	-2.00	-1.60	-1.20	-0.80	-0.40
10^{-6}	-9.15	-7.44	-6.20	-5.53	-4.66	-3.90	-2.80	-2.00	-1.60	-1.20	-0.80	-0.40

Table 1: Slopes of the plots $\ln(m^{-2}\rho_-(r))$ vs. $\ln(r/r_0)$. The slope describes the linear behavior present in the curves shown, for instance, in figure 4; we considered different values for the charge of the impurity n. While the slope takes the value $\Gamma_n = -n\beta e^2 = -2n$ for $n < 1$ and $r_0 \to 0$, the slope does not satisfy this relation as $n > 1$ or r_0 is large enough. The larger n the lesser the slope approximates to $-2n$. For $n = 1$ the slope also satisfies this condition. Our results match the predictions stated in [23] found when $\Gamma < 2$ and $r_0 \to 0$. We used $m^{-2}\rho^0 = 0.87$ and $mR = 30$.

we find

$$\frac{2\pi}{m^2}\rho_+^{(\nu_+,\tilde{r}_0,\infty)}(\mathbf{r}) = \frac{2\pi}{m^2}\tilde{\rho}_\nu^0 - \sum_{l=1}^{\infty}[t_{l-\nu}^{(0)}]^{-1}[K_{l-\nu}^{(r)}]^2 - \sum_{l=0}^{k-1}[t_{l+\nu}^{(0)}]^{-1}[K_{l+\nu}^{(r)}]^2 + \sum_{l=k}^{\infty}[t_{l+\nu+1}^{(0)}]^{-1}[K_{l+\nu}^{(r)}]^2, \tag{44}$$

$$\frac{2\pi}{m^2}\rho_-^{(\nu_+,\tilde{r}_0,\infty)}(\mathbf{r}) = \frac{2\pi}{m^2}\tilde{\rho}_\nu^0 + \sum_{l=1}^{\infty}[t_{l-\nu+1}^{(0)}]^{-1}[K_{l-\nu}^{(r)}]^2 + \sum_{l=0}^{k}[t_{l+\nu-1}^{(0)}]^{-1}[K_{l+\nu}^{(r)}]^2 - \sum_{l=k+1}^{\infty}[t_{l+\nu}^{(0)}]^{-1}[K_{l+\nu}^{(r)}]^2. \tag{45}$$

Finally, we can combine both limits $r_0 \to 0$ and $R \to \infty$. In the interval $r_0 \ll r \ll R$ we get

$$\rho_+^{(\nu_+,0,\infty)}(\mathbf{r}) = \tilde{\rho}_\nu^0 - \left(\frac{m^2}{2\pi}\right)^2 \frac{(1-\delta_{0k})\delta_{0\nu}}{\rho^0(r_0)}[K_0^{(r)}]^2, \tag{46}$$

$$\rho_-^{(\nu_+,0,\infty)}(\mathbf{r}) = \tilde{\rho}_\nu^0 + \left(\frac{m^2}{2\pi}\right)^2 \frac{(1-\delta_{0k})\delta_{0\nu}}{\rho^0(r_0)}[K_1^{(r)}]^2 + \frac{m^2}{2\pi}d_\nu^0[K_\nu^{(r)}]^2. \tag{47}$$

mr_0	n								
	7	5.3	3.5	2	1	0.7	0.5	0.3	0.1
10^{-1}	6.51	5.91	5.01	3.66	1.94	1.15	0.586	3.76×10^{-2}	-0.464
10^{-2}	11.1	10.5	9.55	8.16	5.82	4.11	2.75	1.37	7.11×10^{-3}
10^{-3}	15.7	15.1	14.2	12.7	10.0	7.29	5.07	2.82	0.607
10^{-4}	20.3	19.7	18.8	17.3	14.4	10.5	7.37	4.23	1.22
10^{-5}	24.9	24.3	23.4	21.9	18.7	13.7	9.67	5.62	1.80
10^{-6}	29.5	28.9	28.0	26.6	23.2	16.9	12.0	7.01	2.34
10^{-7}	34.1	33.5	32.6	31.1	27.6	20.2	14.3	8.39	2.87
10^{-8}	38.7	38.1	37.2	35.7	32.1	23.4	16.6	9.77	3.37
10^{-9}	43.3	42.8	41.8	40.3	36.6	26.6	18.9	11.2	3.87
10^{-10}	48.0	47.4	46.4	44.9	41.1	29.8	21.2	12.5	4.35

Table 2: Value of $\ln(m^{-2}\rho_-(r))$ at $r = r_0$ for different values of r_0 and n. As expected, the smaller r_0, the larger the negative density at $r = r_0$ because the collapse of the counter-ions is stronger. For $n > 1$ the values of the negative density at r_0 take a very large value as $r_0 \to 0$. For $n < 1$ such values are also large but notably decrease because of the decrease of negative ions already described. We used $m^{-2}\rho^0 = 0.87$ and $mR = 30$.

From Eqs. (46) and (47) we can obtain the particular cases

$$\rho_+^{(\nu_+,0,\infty)}(\mathbf{r}) = \begin{cases} \rho^0, & n = 0 \\ \frac{\rho_{++}^{(2)0}(r,0)}{\rho^0(r_0)}, & n \geq 1, n \in \mathbb{Z} \\ \tilde{\rho}_\nu^0, & n \notin \mathbb{Z} \end{cases} \tag{48}$$

$$\rho_-^{(\nu_+,0,\infty)}(\mathbf{r}) = \begin{cases} \rho^0, & n = 0 \\ \frac{\rho_{+-}^{(2)0}(r,0)}{\rho^0(r_0)}, & n \geq 1, n \in \mathbb{Z} \\ \tilde{\rho}_\nu^0 + \frac{m^2}{2\pi} d_\nu^0 [K_\nu^{(r)}]^2, & n \notin \mathbb{Z} \end{cases} \tag{49}$$

where $\rho_{+\pm}^{(2)0}(r,0)$ are the two-point correlation functions for the unperturbed plasma [1]. Notice that for $n \geq 1$ and $n \in \mathbb{Z}$ both the positive and negative densities do not depend on n (their respective densities are the same for any integer charge). This takes place because an amount of $k-1$ counter-ions screen the impurity as their collapse cannot be avoided in the limit $r_0 \to 0$ leaving a charge $n = 1$ unscreened.

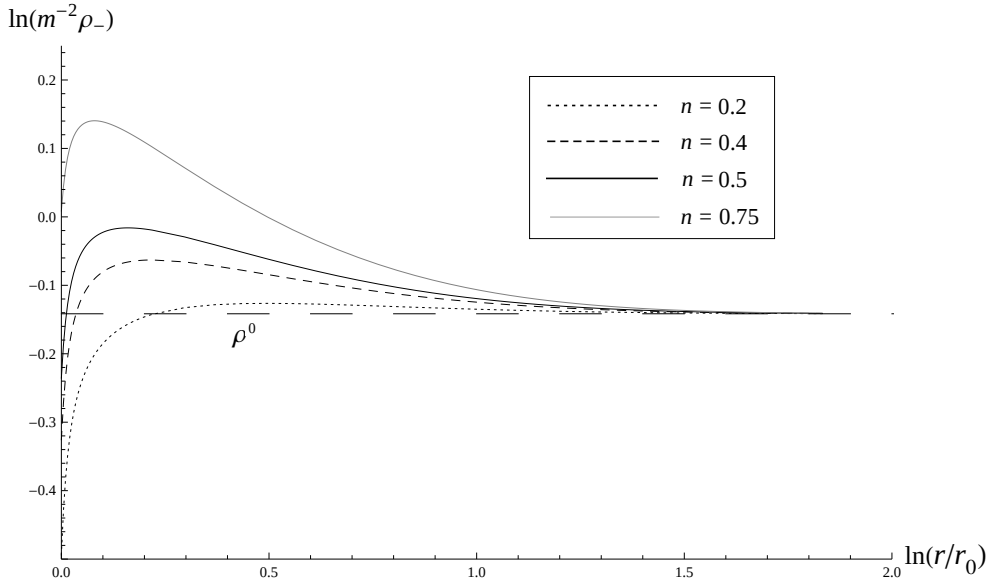

Figure 5: Density of the negative charge for four different fractional impurities located at the origin. The size of the impurity is $mr_0 = 0.4$ and the size of the disk is $mR = 30$. Notice that the negative density close to the impurity decreases due to the reduction of counter-ions when r_0 increases. A large impurity avoids the strong collapse of counter-ions due to its hard core effects; this effect does not occur as $r_0 \to 0$. We used $m^{-2}\rho^0 = 0.87$.

5 Integrated Charge

We now focus on finding the integrated charge of the system contained in an annulus region from r_0 up to a distance $r > r_0$. Let $e_\pm(r, r_0) = \int_{r_0}^{r}\int_0^{2\pi} \rho_\pm(\mathbf{r}) d^2r$. We now define the following functions

$$a_j(r, r_0) = \frac{m^2}{2\pi}\int_{r_0}^{r}\int_0^{2\pi} d^2r' [K_j^{(r')}]^2 = \frac{x^2}{2}\Big[[\, K_j^{(x)}]^2 - K_{j-1}^{(x)} K_{j+1}^{(x)}\Big]\Big|_{\tilde{r}_0}^{\tilde{r}}, \tag{50}$$

$$b_j(r, r_0) = \frac{m^2}{2\pi}\int_{r_0}^{r}\int_0^{2\pi} d^2r' [\, I_j^{(r')}]^2 = \frac{x^2}{2}\Big[[I_j^{(x)}]^2 - I_{j-1}^{(x)} I_{j+1}^{(x)}\Big]\Big|_{\tilde{r}_0}^{\tilde{r}}, \tag{51}$$

$$c_j(r, r_0) = \frac{m^2}{2\pi}\int_{r_0}^{r}\int_0^{2\pi} d^2r' I_j^{(r')} K_j^{(r')}, \tag{52}$$

$$e_0(r, r_0) = \int_{r_0}^{r}\int_0^{2\pi} d^2r' \rho^0 = \frac{\tilde{r}^2 - \tilde{r}_0^2}{2}\left(\ln\frac{2}{ma} - \gamma\right). \tag{53}$$

The total positive and negative charges in the annulus region can easily be found by integrating the densities found in the previous section and using Eqs. (50)–(53). The

integrated charge, from r_0 up to a distance r, is given by $e_t(r,r_0) = \int_{r_0}^{r}\int_0^{2\pi} d^2r'(\rho_+(r') - \rho_-(r'))$. Its general expression is given by

$$\begin{aligned}
e_t^{(\nu_+,\tilde{r}_0,\tilde{R})}(r) = &-\sum_{l=0}^{k-1}\frac{[t_{l+\nu}^{(0)}]^{-1}A_{l+\nu}(r,r_0)}{1+[t_{l+\nu}^{(0)}]^{-1}t_{l+\nu+1}^{(R)}} - \sum_{l=0}^{k-1} t_{l+\nu+1}^{(R)}\frac{2[t_{l+\nu}^{(0)}]^{-1}C_{l+\nu}(r,r_0) - B_{l+\nu}(r,r_0)}{1+[t_{l+\nu}^{(0)}]^{-1}t_{l+\nu+1}^{(R)}} \\
&-\sum_{l=1}^{\infty}\frac{[t_{l-\nu+1}^{(0)}]^{-1}A_{l-\nu}(r,r_0)}{1+[t_{l-\nu+1}^{(0)}]^{-1}t_{l-\nu}^{(R)}} + \sum_{l=1}^{\infty} t_{l-\nu}^{(R)}\frac{2[t_{l-\nu+1}^{(0)}]^{-1}C_{l-\nu}(r,r_0) + B_{l-\nu}(r,r_0)}{1+[t_{l-\nu+1}^{(0)}]^{-1}t_{l-\nu}^{(R)}} \\
&+\sum_{l=k}^{\infty}\frac{[t_{l+\nu+1}^{(0)}]^{-1}A_{l+\nu}(r,r_0)}{1+[t_{l+\nu+1}^{(0)}]^{-1}t_{l+\nu}^{(R)}} - \sum_{l=k}^{\infty} t_{l+\nu}^{(R)}\frac{2[t_{l+\nu+1}^{(0)}]^{-1}C_{l+\nu}(r,r_0) + B_{l+\nu}(r,r_0)}{1+[t_{l+\nu+1}^{(0)}]^{-1}t_{l+\nu}^{(R)}} \\
&-\frac{[t_{\nu-1}^{(0)}]^{-1}a_{\nu}(r,r_0)}{1+[t_{\nu-1}^{(0)}]^{-1}t_{\nu}^{(R)}} + t_{\nu}^{(R)}\frac{2[t_{\nu-1}^{(0)}]^{-1}c_{\nu}(r,r_0) + b_{\nu}(r,r_0)}{1+[t_{\nu-1}^{(0)}]^{-1}t_{\nu}^{(R)}} \\
&-\frac{[t_{1-\nu}^{(0)}]^{-1}a_{1-\nu}(r,r_0)}{1+[t_{1-\nu}^{(0)}]^{-1}t_{-\nu}^{(R)}} - t_{-\nu}^{(R)}\frac{2[t_{1-\nu}^{(0)}]^{-1}c_{1-\nu}(r,r_0) - b_{1-\nu}(r,r_0)}{1+[t_{1-\nu}^{(0)}]^{-1}t_{-\nu}^{(R)}}
\end{aligned} \tag{54}$$

where we used the definitions

$$a_{l+\nu}(r,r_0) + a_{l+\nu+1}(r,r_0) = -xK_{l+\nu}^{(x)}K_{l+\nu+1}^{(x)}\Big|_{r_0}^{r} \equiv A_{l+\nu}(r,r_0), \tag{55}$$

$$b_{l+\nu}(r,r_0) + b_{l+\nu+1}(r,r_0) = xI_{l+\nu}^{(x)}I_{l+\nu+1}^{(x)}\Big|_{r_0}^{r} \equiv B_{l+\nu}(r,r_0), \tag{56}$$

$$c_{l+\nu}(r,r_0) - c_{l+\nu+1}(r,r_0) \equiv C_{l+\nu}(r,r_0). \tag{57}$$

5.1 Integrated Charge at the boundary

An interesting fact is evaluating the total integrated charge at the boundary of the system, i.e., at $r = R$. We should expect this charge to vanish because, excluding the impurity, the system is neutral. We can easily check that in the limits $\tilde{R} \gg 1$ and $\tilde{r}_0 \ll 1$ we have

$$A_{l+\nu}(R,r_0) = \tilde{r}_0 K_{l+\nu+1}(\tilde{r}_0)K_{l+\nu}(\tilde{r}_0) + O(e^{-\tilde{R}}), \tag{58}$$

$$B_{l+\nu}(R,r_0) = \tilde{R} I_{l+\nu+1}(\tilde{R})I_{l+\nu}(\tilde{R}) + O(\tilde{r}_0^{2(l+\nu+1)}). \tag{59}$$

Since $t_{l+\nu+1}^{(R)} \sim e^{-2\tilde{R}}$, the contributions coming from the terms $C_l(R,r_0)$ are exponentially small and so can be neglected. We thus have

$$\begin{aligned}
e_t^{(\nu_+,\tilde{r}_0,\tilde{R})}(R) = &-\sum_{l=1}^{\infty}\frac{\tilde{r}_0 I_{l-\nu+1}^{(0)}K_{l-\nu}^{(0)}}{1+[t_{l-\nu+1}^{(0)}]^{-1}t_{l-\nu}^{(R)}} - \sum_{l=0}^{k-1}\frac{\tilde{r}_0 I_{l+\nu}^{(0)}K_{l+\nu+1}^{(0)}}{1+[t_{l+\nu}^{(0)}]^{-1}t_{l+\nu+1}^{(R)}} + \sum_{l=k}^{\infty}\frac{\tilde{r}_0 I_{l+\nu+1}^{(0)}K_{l+\nu}^{(0)}}{1+[t_{l+\nu+1}^{(0)}]^{-1}t_{l+\nu}^{(R)}} \\
&+\sum_{l=1}^{\infty}\frac{\tilde{R}K_{l-\nu}^{(R)}I_{l-\nu+1}^{(R)}}{1+[t_{l-\nu+1}^{(0)}]^{-1}t_{l-\nu}^{(R)}} + \sum_{l=0}^{k-1}\frac{\tilde{R}K_{l+\nu+1}^{(R)}I_{l+\nu}^{(R)}}{1+[t_{l+\nu}^{(0)}]^{-1}t_{l+\nu+1}^{(R)}} - \sum_{l=k}^{\infty}\frac{\tilde{R}K_{l+\nu}^{(R)}I_{l+\nu+1}^{(R)}}{1+[t_{l+\nu+1}^{(0)}]^{-1}t_{l+\nu}^{(R)}} \\
&-\frac{\tilde{r}_0 I_{1-\nu}^{(0)}K_{\nu}^{(0)} + d_{\nu}^{0}a_{\nu}(R,r_0)}{1+t_{\nu}^{(R)}(d_{\nu}^{0}+[t_{1-\nu}^{(0)}]^{-1})} + \frac{\tilde{R}K_{\nu}^{(R)}I_{1-\nu}^{(R)}}{1+t_{\nu}^{(R)}(d_{\nu}^{0}+[t_{1-\nu}^{(0)}]^{-1})} + O(e^{-\tilde{R}}, \tilde{r}_0^{2(l+1)}).
\end{aligned} \tag{60}$$

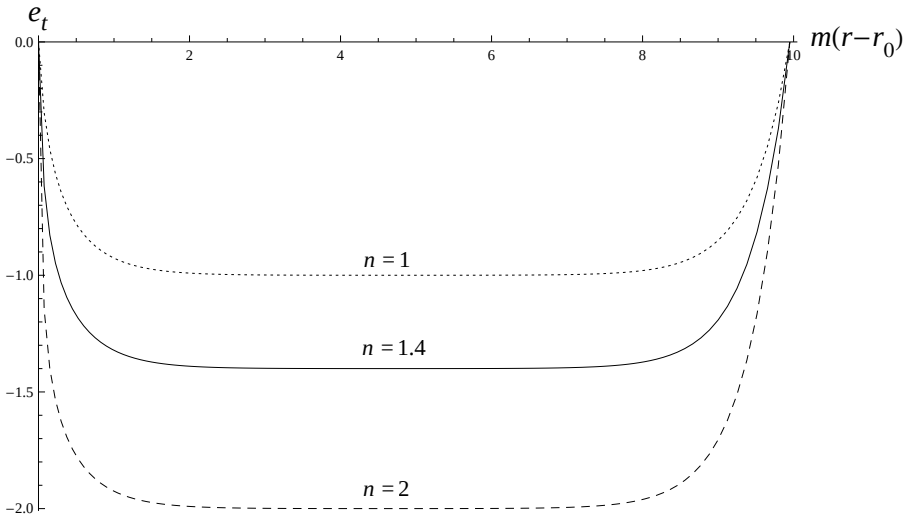

Figure 6: Integrated charge in the plasma for three different impurities located at the origin. The size of the impurity is $mr_0 = 0.05$ and the size of the disk is $mR = 10$.

In the same approximation all the denominators behave like $\sim \frac{1}{1+O(e^{-\tilde{R}})} = 1 + O(e^{-\tilde{R}})$. So

$$\begin{aligned} e_t^{(\nu_+,\tilde{r}_0,\tilde{R})}(R) = & -\tilde{r}_0 \sum_{l=0}^{k-1} \left[I^{(0)}_{l-\nu+1} K^{(0)}_{l-\nu} + I^{(0)}_{l+\nu} K^{(0)}_{l+\nu+1} \right] + \tilde{r}_0 \sum_{l=k}^{\infty} \left[I^{(0)}_{l+\nu+1} K^{(0)}_{l+\nu} - I^{(0)}_{l-\nu+1} K^{(0)}_{l-\nu} \right] \\ & + \tilde{R} \sum_{l=0}^{k-1} \left[K^{(R)}_{l-\nu} I^{(R)}_{l-\nu+1} + K^{(R)}_{l+\nu+1} I^{(R)}_{l+\nu} \right] - \tilde{R} \sum_{l=k}^{\infty} \left[K^{(R)}_{l+\nu} I^{(R)}_{l+\nu+1} - K^{(R)}_{l-\nu} I^{(R)}_{l-\nu+1} \right] \\ & - d^0_\nu a_\nu(R, r_0) + O(e^{-\tilde{R}}, \tilde{r}_0^{2(l+1)}). \end{aligned} \tag{61}$$

When $\nu = 0$, it is easy to see, using the Wronskian relations for the Bessel functions [24], that $e_{t^+}^{(0,\tilde{r}_0,\tilde{R})}(R) = 0$, so the total charge of the system is ne (the charge of the impurity). This means that the charge distribution generated by the impurity close to the origin is compensated by a charge distribution of opposite sign in the boundary. For $\nu \neq 0$ the charge at $r = R$ does not simplify and so numerical solutions must be found; in this case we also find $e_t^{(\nu,\tilde{r}_0,\tilde{R})}(R) = 0$.

Figures 6 and 7 show the integrated charge for different values of the impurity charge n. By definition it starts with a zero value at $r = r_0 \neq 0$. Then it decreases to reach a valley with a value approaching $-n$ as expected since the plasma screens the impurity. Then, close the outer boundary ($r \to R$), the integrated charge increases to reach the zero value, as discussed above.

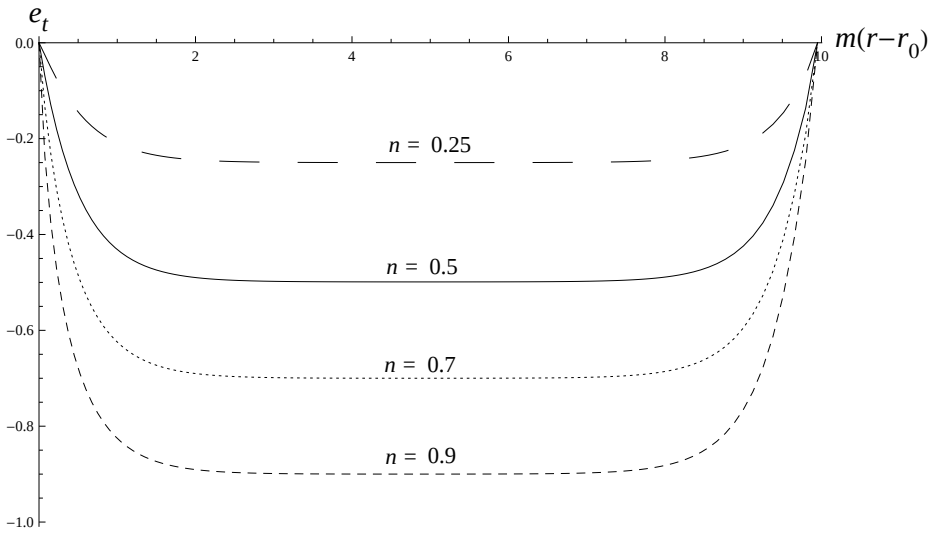

Figure 7: Integrated charge in the plasma for four different impurities located at the origin. The size of the impurity is $mr_0 = 0.05$ and the size of the disk is $mR = 10$.

5.2 Asymptotic Limits

We will evaluate the same asymptotic cases than those analyzed in section 4. For $r_0 \to 0$ and $r \gg r_0$ the net density becomes

$$\begin{aligned} e_t^{(\nu_+,0,\tilde{R})}(r) = &- k + \delta_{0\nu}\left(1 - \frac{1}{1 + \frac{m^2}{2\pi}\frac{\delta_{0\nu}}{\rho^0(r_0)}t_{1+\nu}^{(R)}}\right) - (1-\delta_{0k})t_{1+\nu}^{(R)}\frac{\frac{2m^2}{2\pi}\frac{\delta_{0\nu}}{\rho^0(r_0)}C_0(r,0) - B_\nu(r,0)}{1 + \frac{m^2}{2\pi}\frac{\delta_{0\nu}}{\rho^0(r_0)}t_{1+\nu}^{(R)}} \\ &+ r\sum_{l=1}^{k-1} t_{l+\nu+1}^{(R)} I_{l+\nu+1}^{(r)} I_{l+\nu}^{(r)} + r\sum_{l=1}^{\infty} t_{l-\nu}^{(R)} I_{l-\nu+1}^{(r)} I_{l-\nu}^{(r)} - r\sum_{l=k}^{\infty} t_{l+\nu}^{(R)} I_{l+\nu+1}^{(r)} I_{l+\nu}^{(r)} \\ &- \frac{d_\nu^0 a_\nu(r,0)}{1 + d_\nu^0 t_\nu^{(R)}} + t_\nu^{(R)}\frac{2d_\nu^0 c_\nu(r,0) + b_\nu(r,0) + b_{1-\nu}(r,0)}{1 + d_\nu^0 t_\nu^{(R)}} \end{aligned} \tag{62}$$

When $R \to \infty$ and $r \ll R$ we have

$$\begin{aligned} e_t^{(\nu_+,\tilde{r}_0,\infty)}(r) = &- \sum_{l=0}^{k-1}[t_{l+\nu}^{(0)}]^{-1} A_{l+\nu}(r,r_0) - \sum_{l=1}^{\infty}[t_{l-\nu+1}^{(0)}]^{-1} A_{l-\nu}(r,r_0) \\ &+ \sum_{l=k}^{\infty}[t_{l+\nu+1}^{(0)}]^{-1} A_{l+\nu}(r,r_0) - [t_{\nu-1}^{(0)}]^{-1} a_\nu(r,r_0) - [t_{1-\nu}^{(0)}]^{-1} a_{1-\nu}(r,r_0) \end{aligned} \tag{63}$$

In the combined limits $r_0 \to 0$ and $R \to \infty$, we get, in the interval $r_0 \ll r \ll R$

$$e_t^{(\nu_+,0,\infty)}(r) = - k - d_\nu^0 a_\nu(r,0) \tag{64}$$

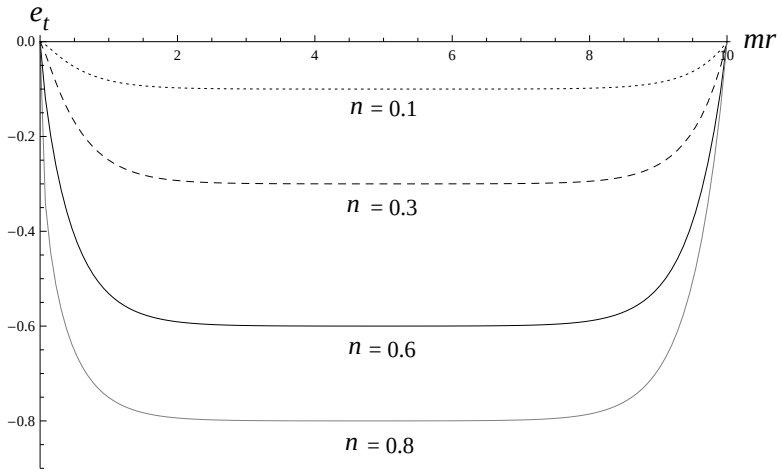

Figure 8: Integrated charge in the plasma for four different fractional impurities located at the origin. The impurity is a treated as point particle ($r_0 = 0$) according to Eq. (62). The size of the disk is $mR = 10$.

Figs. 8 and 9 show the integrated charge in the case when $r_0 = 0$. Fig. 8 is, in essence, similar to Fig. 7 when $r_0 \neq 0$. However, Fig. 9 shows a new interesting effect, which is not present in the case when $r_0 \neq 0$ (Fig. 6). When n is an integer, the accumulated charge $e_t(r)$ starts at $r = r_0 = 0$ with a value equal to $-n$, instead of zero, as it was the case when $r_0 \neq 0$. This means that exactly n ions of charge $-e$ of the plasma (counter-ions) have collapsed at the position $r_0 = 0$ where the impurity is, and they have completely neutralized it. On the other hand, when $n = k + \nu$ is not an integer ($\nu \neq 0$), k negative ions will partially neutralize the impurity by collapsing into it at position $r_0 = 0$, but a fractional charge $e\nu$ remains to be screened, which cannot be completely neutralized by collapsing into it, because the charges of ions the plasma are integers. Nevertheless, this remaining charge is screened by a difuse layer of plasma ions, of tipical length given by the screening length m^{-1}. This situation is illustrated with the cases $n = 1.7$ and $n = 2.4$ in Fig. 9.

Fig. 10 shows the integrated charge for $r_0 \neq 0$ and $R \to \infty$. Since the boundary of the large disk R is now at infinity, the difuse layer of remaining charge that usually accumulates close that boundary, observed in the previous figures, is now receded to infinity with the boundary and it cannot be observed anymore in Fig. 10. Fig. 11 shows the combined effects of taking $r_0 = 0$ and $R \to \infty$.

6 Grand Potential and Pressure

In this section we will calculate the grand potential and the partition function for the system we have discussed. Using Eq. (3) we see that the eigenvectors that generate the

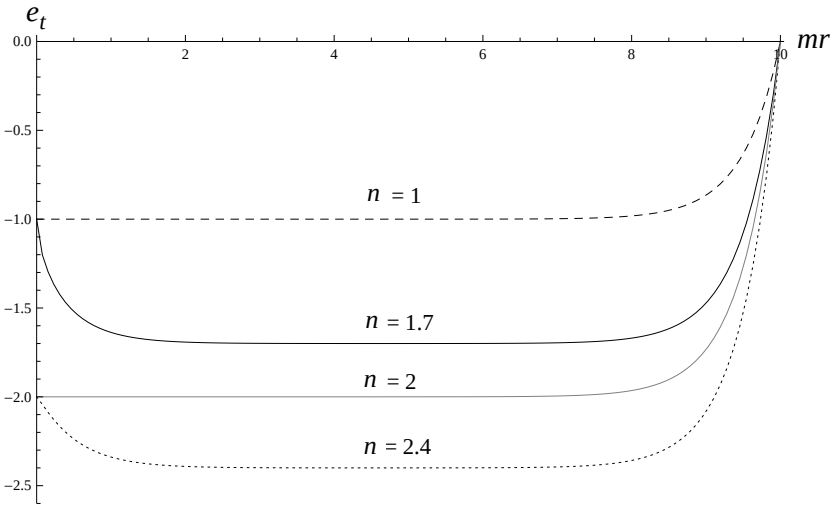

Figure 9: Integrated charge in the plasma for four different impurities located at the origin. The impurity is a treated as point particle ($r_0 = 0$) according to Eq. (62). The size of the disk is $mR = 10$.

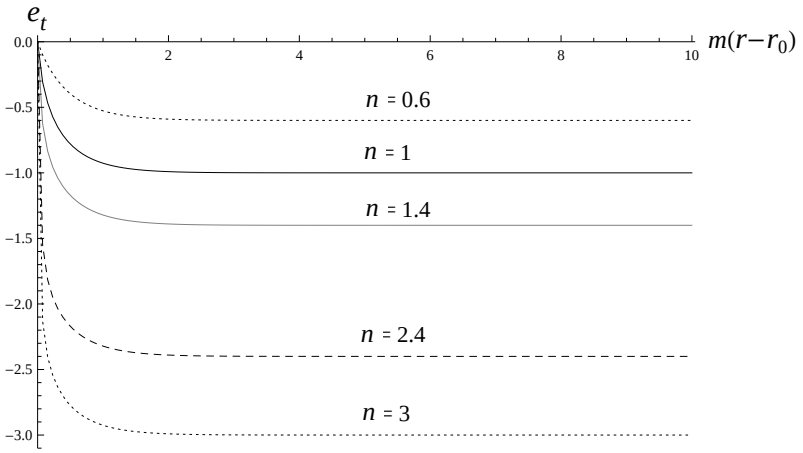

Figure 10: Integrated charge in the plasma for five different impurities located at the origin. The impurity has a size $mr_0 = 0.05$ and we consider the limit $R \to \infty$ according to Eq. (63). The density of the gas is constant with value $-n$ for large enough distances.

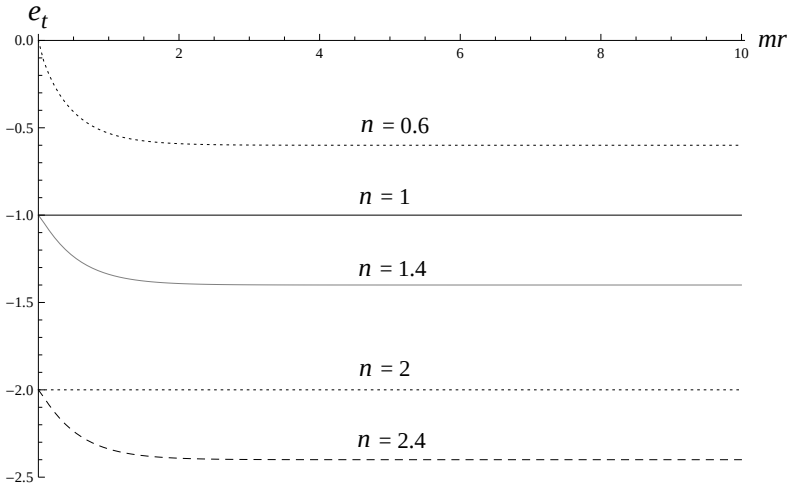

Figure 11: Integrated charge in the plasma for five different impurities located at the origin. We consider the limits $r_0 \to 0$ and $R \to \infty$ according to Eq. (64).

partition function satisfy the equations

$$\begin{aligned} m_+(\mathbf{r})g(\mathbf{r}) &= 2\lambda\partial_z f(\mathbf{r}), \\ m_-(\mathbf{r})f(\mathbf{r}) &= 2\lambda\partial_{\bar{z}} g(\mathbf{r}). \end{aligned} \tag{65}$$

Remember that for this problem $m_\pm(\mathbf{r}) = m(\mathbf{r})\left(\frac{r}{L}\right)^{\pm 2n}$, where

$$m(\mathbf{r}) \;\; = \;\; \left\{ \begin{array}{l} 0, \;\; r < r_0 \\ m, \;\; r > r_0 \end{array} \right. . \tag{66}$$

In the region $r_0 < r < R$ it is more convenient to define the functions $\bar{g}(\mathbf{r}) = e^{-V(\mathbf{r})}g(\mathbf{r})$ and $\bar{f}(\mathbf{r}) = e^{V(\mathbf{r})}f(\mathbf{r})$. Decomposing $\bar{g}(\mathbf{r})$ as a Fourier series of the form $\bar{g}_l(\mathbf{r}) = \bar{g}_l(r)e^{il\theta}$, we find each mode satisfies the differential equation

$$\left\{ \rho^2 \frac{d^2}{d\rho^2} + \rho\frac{d}{d\rho} - \left[(l+n)^2 + \rho^2 \right] \right\} \bar{g}_l(\rho) = 0, \tag{67}$$

with $\rho \equiv \frac{\tilde{r}}{\lambda}$. The general solutions are given by

$$\begin{aligned} g_l(\mathbf{r}) &= \left(\frac{r}{L}\right)^{-n} e^{il\theta}\Big(B_l I_{l+n}(\rho) + A_l K_{l+n}(\rho) \Big), \\ f_l(\mathbf{r}) &= \left(\frac{r}{L}\right)^{n} e^{i(l+1)\theta}\Big(B_l I_{l+n+1}(\rho) - A_l K_{l+n+1}(\rho) \Big). \end{aligned} \tag{68}$$

In the first region ($r < r_0$) and the third region ($r > R$), we have the general solutions

$$g_l^{(1,3)}(\mathbf{r}) = u_l^{(1,3)} e^{il\theta}\left(\frac{mL}{\lambda}\right)^n \left(\frac{\tilde{r}}{\lambda}\right)^l, \tag{69}$$

$$f_l^{(1,3)}(\mathbf{r}) = v_l^{(1,3)} e^{i(l+1)\theta}\left(\frac{\lambda}{mL}\right)^n \left(\frac{\tilde{r}}{\lambda}\right)^{-l-1}. \tag{70}$$

(The coefficients 1, 3 refer to the first and third regions.) The boundary conditions imply again that both $g_l^{(1)}(\mathbf{r})$ and $f_l^{(1)}(\mathbf{r})$ must be finite at $r = 0$ while $g_l^{(3)}(\mathbf{r})$ and $f_l^{(3)}(\mathbf{r})$ must vanish at $r \to \infty$. This generates the conditions

$$\begin{pmatrix} -K_{l+n+1}(\tilde{r}_0/\lambda) & I_{l+n+1}(\tilde{r}_0/\lambda) \\ K_{l+n}(\tilde{R}/\lambda) & I_{l+n}(\tilde{R}/\lambda) \end{pmatrix} \begin{pmatrix} A_l \\ B_l \end{pmatrix} = \begin{pmatrix} 0 \\ 0 \end{pmatrix} \tag{71}$$

for $l \geq 0$, and

$$\begin{pmatrix} K_{l+n}(\tilde{r}_0/\lambda) & I_{l+n}(\tilde{r}_0/\lambda) \\ -K_{l+n+1}(\tilde{R}/\lambda) & I_{l+n+1}(\tilde{R}/\lambda) \end{pmatrix} \begin{pmatrix} A_l \\ B_l \end{pmatrix} = \begin{pmatrix} 0 \\ 0 \end{pmatrix} \tag{72}$$

for $l \leq -1$. The solutions are non-vanishing if the determinant of previous matrices is zero. Thus, we have the conditions (after shifting indices and defining $z = \lambda^{-1}$)

$$K_{l+n+1}(\tilde{r}_0 z)I_{l+n}(\tilde{R}z) + K_{l+n}(\tilde{R}z)I_{l+n+1}(\tilde{r}_0 z) = 0, \quad l \geq 0, \tag{73}$$
$$K_{l+n-1}(\tilde{r}_0 z)I_{l+n}(\tilde{R}z) + K_{l+n}(\tilde{R}z)I_{l+n-1}(\tilde{r}_0 z) = 0, \quad l \leq 0. \tag{74}$$

We now again write n as $n = k + \nu$, with $k \in \mathbb{Z}$ and $|\nu| < 1$. Our conditions now become

$$K_{l+\nu+1}(\tilde{r}_0 z)I_{l+\nu}(\tilde{R}z) + K_{l+\nu}(\tilde{R}z)I_{l+\nu+1}(\tilde{r}_0 z) = 0, \quad l \geq k, \tag{75}$$
$$K_{l-\nu+1}(\tilde{r}_0 z)I_{-l+\nu}(\tilde{R}z) + K_{l-\nu}(\tilde{R}z)I_{-l+\nu-1}(\tilde{r}_0 z) = 0, \quad l \geq -k. \tag{76}$$

After eliminating the negative l-modes in favor of the positive ones we obtain

$$K_{l+|\nu|+1}(\tilde{r}_0 z)I_{l+|\nu|}(\tilde{R}z) + K_{l+|\nu|}(\tilde{R}z)I_{l+|\nu|+1}(\tilde{r}_0 z) = 0, \quad l \geq |k| \tag{77}$$
$$K_{l+|\nu|-1}(\tilde{r}_0 z)I_{l+|\nu|}(\tilde{R}z) + K_{l+|\nu|}(\tilde{R}z)I_{l+|\nu|-1}(\tilde{r}_0 z) = 0, \quad |k| \geq l \geq 0 \tag{78}$$
$$K_{l-|\nu|+1}(\tilde{r}_0 z)I_{l-|\nu|}(\tilde{R}z) + K_{l-|\nu|}(\tilde{R}z)I_{l-|\nu|+1}(\tilde{r}_0 z) = 0, \quad l \geq 1 \tag{79}$$

From now on we will assume $\nu > 0$ and $k > 0$. Let us define the functions

$$h_l^{(1)}(z) = \frac{\tilde{r}_0^{l+\nu+1} z}{\tilde{R}^{l+\nu}} \Big[K_{l+\nu+1}(\tilde{r}_0 z)I_{l+\nu}(\tilde{R}z) + K_{l+\nu}(\tilde{R}z)I_{l+\nu+1}(\tilde{r}_0 z) \Big], \quad l \geq k, \tag{80}$$

$$h_l^{(2)}(z) = \frac{\tilde{R}^{l+\nu} z}{\tilde{r}_0^{l+\nu-1}} \Big[K_{l+\nu-1}(\tilde{r}_0 z)I_{l+\nu}(\tilde{R}z) + K_{l+\nu}(\tilde{R}z)I_{l+\nu-1}(\tilde{r}_0 z) \Big], \quad k \geq l \geq 0, \tag{81}$$

$$h_l^{(3)}(z) = \frac{\tilde{r}_0^{l-\nu+1} z}{\tilde{R}^{l-\nu}} \Big[K_{l-\nu+1}(\tilde{r}_0 z)I_{l-\nu}(\tilde{R}z) + K_{l-\nu}(\tilde{R}z)I_{l-\nu+1}(\tilde{r}_0 z) \Big], \quad l \geq 1. \tag{82}$$

Using the well known properties of the Bessel functions [24], we can check the conditions $h_l^{(i)}(0) = 1$, $h_l'^{(i)}(0) = 0$, and $h_l^{(i)}(z) = h_l^{(i)}(-z)$. As similarly as performed in [1, 10, 11, 12], those properties allow us to decompose our grand potential as a Weierstrass product over its zeroes. The grand potential for our system is

$$\beta\Omega = -\sum_{i=1}^{3} \sum_{l} \ln h_l^{(i)}(-1), \tag{83}$$

where l lies in the intervals $[k,\infty)$, $[0,k]$, and $[1,\infty)$ for $i=1,2$, and 3, respectively.

Therefore, we get

$$\beta\Omega = \beta\Omega_0 + \beta\Omega(n,\tilde{R}) + \beta\Omega(k,\nu,\tilde{r}_0) + \beta\Omega^{\nu}(\tilde{R}) + O(e^{-2\tilde{R}}), \tag{84}$$

where [1]

$$\beta\Omega_0 = -\pi R^2\,\frac{m^2}{2\pi}\Big[\ln\tfrac{2}{ma} - \gamma + \tfrac{1}{2}\Big] + 2\pi R\,m\Big[\tfrac{1}{4} - \tfrac{1}{2\pi}\Big] + \tfrac{1}{6}\ln(mR) + O(1) \tag{85}$$

is the grand potential of the unperturbed plasma, and (remember that $k+\nu=n$)

$$\beta\Omega(n,\tilde{R}) = n\ln(mR) - \ln[\,\Gamma(n+1)\,] - n\ln 2 + O(1/\tilde{R}), \tag{86}$$

$$\begin{aligned}\beta\Omega(k,\nu\,,\tilde{r}_0) = &-\sum_{l=k}^{\infty}\ln\left[\left(\frac{\tilde{r}_0}{2}\right)^{l+\nu+1}\frac{2\,K^{(0)}_{l+\nu+1}}{\Gamma(l+\nu+1)}\right] - \sum_{l=1}^{\infty}\ln\left[\left(\frac{\tilde{r}_0}{2}\right)^{l-\nu+1}\frac{2\,K^{(0)}_{l-\nu+1}}{\Gamma(l-\nu+1)}\right]\\ &-\sum_{l=0}^{k}\ln\left[\frac{\tilde{R}^{2(l+\nu)}}{\tilde{r}_0^{\,l+\nu-1}}\frac{K^{(0)}_{l+\nu-1}}{2^{l+\nu}\Gamma(l+\nu+1)}\right],\end{aligned} \tag{87}$$

$$\begin{aligned}\beta\Omega^{\nu}(\tilde{R}) = &-\sum_{l=0}^{\infty}\ln\left[\frac{I^{(R)}_{l+\nu}}{I^{(R)}_{l}}\frac{\Gamma(l+\nu+1)}{\Gamma(l+1)}\left(\frac{2}{\tilde{R}}\right)^{\nu}\right] - \sum_{l=1}^{\infty}\ln\left[\frac{I^{(R)}_{l-\nu}}{I^{(R)}_{l}}\frac{\Gamma(l-\nu+1)}{\Gamma(l+1)}\left(\frac{2}{\tilde{R}}\right)^{-\nu}\right]\\ &-\ln\left[\frac{I^{(R)}_{\nu}}{I^{(R)}_{0}}\right].\end{aligned} \tag{88}$$

Last expressions cannot be evaluated exactly. For $\tilde{r}_0 \ll 1$ and $\tilde{R} \gg 1$ we can use the Euler Mc-Laurin formula to transform discrete sums into integrals and expand $K^{(0)}_l$ in powers of $\tilde{r}_0$ using the fact that $\tilde{r}_0 \ll 1$. After some algebra, adding all the different contributions so we can write the grand potential as $\beta\Omega = \beta\Omega_0 + \beta\Omega_1(k,\nu)$, and neglecting $O(1)$ terms we find

$$\beta\Omega_1(0,0) = \tfrac{\tilde{r}_0^2}{2}\ln\left(\frac{R}{a}\right) + O(\tilde{r}_0^2\ln\tilde{r}_0), \tag{89}$$

$$\beta\Omega_1(n,0) = -\ln\left[\ln\left(\tfrac{2}{\tilde{r}_0}\right) - \gamma\right] + n(n-1)\ln\tilde{r}_0 - n^2\ln(mR) + \tfrac{\tilde{r}_0^2}{2}\ln\left(\frac{R}{a}\right) + O(\tilde{r}_0^2\ln\tilde{r}_0), \tag{90}$$

and

$$\beta\Omega_1(0,\nu) = -\nu^2\ln(mR) + \tfrac{\tilde{r}_0^2}{2}\ln\left(\frac{R}{a}\right) + O(\tilde{r}_0^{2(1-\nu)}), \tag{91}$$

$$\beta\Omega_1(k,\nu) = \Big[n(n-1) + \nu(1-\nu)\Big]\ln\tilde{r}_0 - n^2\ln(mR) + \tfrac{\tilde{r}_0^2}{2}\ln\left(\frac{R}{a}\right) + O(\tilde{r}_0^{2(1-\nu)},\,\tilde{r}_0^{2\nu}). \tag{92}$$

The results found for the grand potential are consistent with what we expect. First of all, the bulk pressure and the surface tension are not modified by the presence of the impurity, because we are working in the thermodynamic limit and one single impurity cannot alter extensive quantities, or quantities proportional to the boundary length of the system. Second, we expect to find terms proportional to $\ln \tilde{r}_0$ that diverge when $r_0 \to 0$ and increase with n because of the mentioned particle collapse at $\Gamma = 2$. However, notice that such divergence does not appear when $n = 0$ because such condition only applies for charged particles; the only contribution in the case $n = 0$ is a hard core effect that depends on the cutoff a and vanishes as $r_0 \to 0$, Eq. (89), which is expected. Notice that such hard core effect is present for all values of n.

The term proportional to $\ln(mR)$ is a universal finite-size correction term that is related to the topology of the considered system. Generally, for a two-dimensional conformal field theory, confined in a domain of typical length R, in the limit $R \to \infty$, the free energy of the system exhibits a finite size correction given by $\beta\Delta F = -\frac{1}{6}c\chi \ln(R)$, where c is the conformal anomaly number (central charge) and χ the Euler characteristic of the domain containing the system [25]. As explained in [26, 27], Coulomb systems should exhibit a similar correction, with $c = 1$, due to the long range of the electric potential correlations, however with a change of sign, due to the fact that, in the partition function, one integrates over the fluctuations of the density and not directly over the fluctuations of the electric potential. Now, in the present system, we have shown that the finite size correction to the grand potential is changed from $\frac{1}{6}\ln(mR)$ to $\frac{1-6n^2}{6}\ln(mR)$. The presence of the charged impurity modifies the central charge from $c = 1$ to $c = 1 - 6n^2$. This is in agreement with what is expected from conformal field theory, as a simple deformation of the minimal free boson conformal field theory ($c = 1$) is obtained by spreading out a charge $\alpha_0/2 = n$ at infinity to obtain a conformal field theory with $c = 1 - 24\alpha_0^2 = 1 - 6n^2$ [28, 29]. For the Coulomb system studied here, the external charge is not spread at infinity, but located at the origin. Nevertheless it has the same effect of shifting the central charge from $c = 1$ to $c = 1 - 6n^2$.

One difference between the contributions of integer and non-integer charges to the grand potential is in the terms associated with $\ln \tilde{r}_0$. While the term $\Delta\Omega = n(n-1)\ln \tilde{r}_0$ is common in both cases, there is an additional contribution that differs in the integer and the non-integer cases. For integer charges, this contribution is $\beta\Delta\Omega_{int} = -\ln\left[\ln\left(\frac{2}{\tilde{r}_0}\right) - \gamma\right]$, which clearly differs from the contribution for non-integer charges, given by $\beta\Delta\Omega_{non-int} = \nu(1-\nu)\ln \tilde{r}_0$.

7 Conclusions

We have studied a two-dimensional two-component plasma at $\Gamma = 2$ with an electric impurity confined in a large disk of radius R. Particularly, we found analytical expressions for the density and correlation functions and the grand potential, which provide

information for the pressure and the superficial tension. When the impurity is located at the origin of the confined plasma there is rotational invariance and the equations can be solved analytically using the method described in [1]. The counter-ions and co-ions accumulate close to the origin and the boundary respectively.

The case in which the electric charge of the impurity is an integer multiple of the charges in the plasma $\pm e$ and the case where the impurity charge is not an integer multiple of $\pm e$ were analyzed independently, to highlight some interesting differences due to the discrete nature of the electric charges of ions of the plasma. Although we could have expected quite different behaviors in the cases where the charge takes an "integer" and a "non-integer" value, we found that the effects on the charge redistribution are similar when the radius of the impurity $r_0 \neq 0$. But for a point-like impurity, $r_0 = 0$, important differences can be observed between the "integer" and "non-integer" cases. When the impurity charge has an integer value and $r_0 \to 0$ there is an integer number of counter-ions that can cancel such effect when they collapse at the site where the impurity is located. On the other hand, finite-size effects for finite r_0 avoid the cancellation of the charge of the impurity and so the charge is differently redistributed close to the impurity. When $r_0 > 0$ the charges redistribute in such way that there are accumulated charges $-n$ and n around the impurity and the boundary respectively. In the case $r_0 \to 0$, and a non integer value of the charge $n = k + \nu$ ($\nu \neq 0$), k counter-ions collapse into the impurity, and the charge accumulated around the impurity is only $-\nu e$.

This problem can be extended with the introduction of an additional impurity. Unfortunately, the rotational symmetry in this situation is broken and it might not be possible to find analytical results. When two impurities are included, we expect to obtain the effect of each individual particle (ignoring the effects of the other) plus an additional term that is related to the interaction between the two particles.

The results for the grand potential are as expected. Since the size of the impurity is negligible compared to the the size of the disk, we do not expect the pressure and the superficial tension to be modified. Nonetheless, the central charge of the system is modified because of the presence of the impurity. In this case, we found that the topological term takes the form $\left(\frac{1}{6} - n^2\right) \ln(mR)$, with n the charge of the impurity, indicating a change in the central charge from $c = 1$ to $c = 1 - 6n^2$.

Partial financial support from Fondo de Investigaciones, Facultad de Ciencias, Universidad de los Andes (project 2014-2 "Impurezas cargadas en plasmas y electrolitos"), and ECOS-Nord/COLCIENCIAS-MEN-ICETEX is acknowledged.

References

[1] F. Cornu and B. Jancovici, The electrical double layer: A solvable model, *J. Chem. Phys.* **90**:2444 (1989).

[2] L. Šamaj and I. Travěnec, Thermodynamic properties of the two-dimensional two-component plasma, *J. Stat. Phys.* **101**:713 (2000).

[3] L. Šamaj and B. Jancovici, Surface tension of a metal - electrolyte boundary: exactly solvable model, *J. Stat. Phys.* **103**:717 (2001).

[4] L. Šamaj, Surface tension of an ideal dielectric - electrolyte boundary: exactly solvable model, *J. Stat. Phys.* **103**:737 (2001).

[5] J. M. Kosterlitz, D. J. Thouless, Ordering, metastability and phase transitions in two-dimensional systems, *J. Phys. C* **6**:1181 (1973).

[6] P. Kalinay, L. Samaj, Thermodynamic properties of the two-dimensional coulomb gas in the low-density limit, *J. Stat. Phys.* **106**:857-874 (2002).

[7] G. Téllez, Equation of state in the fugacity format for the two-dimensional Coulomb gas, *J. Stat. Phys.* **126**:281 (2007)

[8] M. L. Rosinberg, J. L. Lebowitz, L. Blum, Solvable model for localized adsorption in a Coulomb system, *J. Stat. Phys.* **44**:153 (1986).

[9] F. Cornu, Two-dimensional models for an electrode with adsorption sites, *J. Stat. Phys.* **54**:681 (1989).

[10] G. Téllez, L. Merchán, Solvable model for electrolytic soap films: the two-dimensional two-component plasma, *J. Stat. Phys.* **108**:495 (2002).

[11] L. Merchán, G. Téllez, Confined Coulomb systems with adsorbing boundaries: the two-dimensional two-component plasma, *J. Stat. Phys.* **114**:735 (2004).

[12] A. Ferrero, G. Téllez, Two-dimensional two-component plasma with adsorbing impurities, *J. Stat. Phys.* **129**:759 (2007).

[13] P. Debye and E. Hückel, The theory of electrolytes. I. Lowering of freezing point and related phenomena, *Phys. Z.* **24**:185 (1923).

[14] R. M. Fuoss, A. Katchalsky, S. Lifson, The potential of an infinite rod-like molecule and the distribution of the counter ions, *Proc. Natl Acad. Sci. USA* **37**:579 (1951).

[15] G. S. Manning, Limiting laws and counterion condensation in polyelectrolyte solutions I. Colligative properties, *J. Chem. Phys.* **51**:924 (1969).

[16] I. Rouzina, V. A. Bloomfield, Macroion attraction due to electrostatic correlation between screening counterions. 1. Mobile surface-adsorbed ions and diffuse ion cloud, *J. Phys. Chem.* **100**:9977 (1996).

[17] A. Naji and R.R. Netz, Attraction of like-charged macroions in the strong-coupling limit, *Eur. Phys. J. E* **13**:43 (2004).

[18] A. Naji and S. Jungblut, A.G. Moreira and R.R. Netz, Electrostatic interactions in strongly-coupled soft matter, *Physica A* **352**:131 (2005)

[19] L. Šamaj, E. Trizac, Counterions at highly charged interfaces: From one plate to like-charge attraction, *Phys. Rev. Lett.* **106**:078301 (2011).

[20] L. Šamaj, E. Trizac, Wigner-crystal formulation of strong-coupling theory for counterions near planar charged interfaces, *Phys. Rev. E* **84**:041401 (2011).

[21] J. P. Mallarino, G. Téllez, E. Trizac, Counter-ion density profile around charged cylinders: the strong-coupling needle limit, *J. Phys. Chem. B* **117**:12702 (2013).

[22] L. Šamaj, Anomalous effects of "guest" charges immersed in electrolyte: Exact 2D results, *J. Stat. Phys.* **120**:125 (2005)

[23] G. Téllez, Short-distance expansion of correlation functions for the charge-symmetric two-dimensional two-component plasma: exact results, *J. Stat. Mech.* P10001 (2005).

[24] I. S. Gradshteyn and I. M. Ryzhik, *Table of Integrals, Series, and Products*, Academic Press, Fifth Edition (1994).

[25] J. L. Cardy, I. Peschel, Finite-size dependence of the free energy in two-dimensional critical systems, *Nucl. Phys. B* **300**:377-392 (1988).

[26] B. Jancovici, G. Manificat, C. Pisani, Coulomb systems seen as critical systems: Finite-size effects in two dimensions, *J. Stat. Phys.* **76**:307-329 (1994).

[27] B. Jancovici, G. Téllez, Coulomb systems seen as critical systems: Ideal conductor boundaries, *J. Stat. Phys.* **82**, 609-632 (1996).

[28] Vl. S. Dotsenko, *Serie de cours sur la théorie conforme*, Université de Paris VI - Université de Paris VII (2004).

[29] P. Ginsparg, *Applied conformal field theory*, Les Houches, Session XLIX, Fields, strings and critical phenomena, ed. by E. Brézin and J. Zinn-Justin, Elsevier (1989).